Met. Mater. Int., Vol. 23, No. 4 (2017), pp. 726~735
doi: 10.1007/s12540-017-6691-z

Effect of Different Microstructural Parameters on Hydrogen Induced Cracking in an API X70 Pipeline Steel

M. A. Mohtadi-Bonab[1,*], M. Eskandari[2], R. Karimdadashi[1], and J. A. Szpunar[3]

[1]Department of Mechanical Engineering, University of Bonab, Bonab 5551761167, Iran
[2]Department of Materials Science &Engineering, Faculty of Engineering, Shahid Chamran University of Ahvaz, Ahvaz 83151-61357, Iran
[3]Department of Mechanical Engineering, University of Saskatchewan, Saskatchewan S7N 5A9, Canada

(received date: 1 October 2016 / accepted date: 12 December 2016)

In this study, the surface and cross section of an as-received API X70 pipeline steel was studied by SEM and EDS techniques in order to categorize the shape and morphology of inclusions. Then, an electrochemical hydrogen charging using a mixed solution of 0.2 M sulfuric acid and 3 g/l ammonium thiocyanate has been utilized to create hydrogen cracks in X70 steel. After hydrogen charging experiments, the cross section of this steel has been accurately checked by SEM in order to find out hydrogen cracks. The region of hydrogen cracks was investigated by SEM and EBSD techniques to predict the role of different microstructural parameters involving hydrogen induced cracking (HIC) phenomenon. The results showed that inclusions were randomly distributed in the cross section of tested specimens. Moreover, different types of inclusions in as-received X70 steel were found. However, only inclusions which were hard, brittle and incoherent with the metal matrix, such as manganese sulfide and carbonitride precipitates, were recognized to be harmful to HIC phenomenon. Moreover, HIC cracks propagate dominantly in transgraular manner through differently oriented grains with no clear preferential trend. Moreover, a different type of HIC crack with about 15-20 degrees of deviation from the rolling direction was found and studied by EBSD technique and role of micro-texture parameters on HIC was discussed.

Keywords: inclusion, crystallographic texture, electron backscatter diffraction, energy dispersive spectroscopy, kernel average misorientation

1. INTRODUCTION

Pipeline steels are widely used for transportation of oil and natural gas over long distances. Due to their higher safety and an economical way to carry out such hydrocarbons, the tendency to use pipeline steels has been increased in recent years. Pipeline steels are usually laid in the field and should tolerate high operating pressures. Therefore, they must have high strength and fracture toughness to work in such harsh environments. Moreover, these steels suffer from several failure modes such as stress corrosion cracking (SCC) and hydrogen induced cracking (HIC). In sour oil and gas environments containing hydrogen sulfide, the HIC phenomenon has been recognized as the most important failure mode in pipeline steels. Hydrogen atoms are produced inside the pipe body due to several reasons [1-3]. However, hydrogen atoms are produced inside the pipe due to the surface corrosion of steel at the presence of hydrogen sulfide and accumulated in various structural defects, such as precipitates, inclusions and dislocations. When the critical amount of hydrogen atoms are gathered in such defects, the HIC cracks may initiate and propagate [4-6]. Even though there are several studies about HIC phenomenon in pipeline steels [7-10], the mechanism of failure by HIC has not been fully understood by researchers. Since inclusions play an important role in HIC crack initiation, many works focused on their role in HIC phenomenon. For instance, the effect of inclusions on HIC susceptibility was studied by Hara *et al.* [11] and it was concluded that nonmetallic inclusions can be considered as crack initiation sites. Kim *et al.* [12] observed that the amount of diffused hydrogen through the pipe body has an important role in crack propagation. These researchers also investigated the role of inclusions in crack nucleation in pipeline steels and showed that inclusions of over 20 μm in length with bainitic ferrite structure increase HIC susceptibility. Hejazi *et al.* [14] studied the role of different types of inclusions on HIC susceptibility in pipeline steels and concluded that aluminum oxide, aluminum-calcium-silicon oxide and elongated manganese sulphide can initiate HIC cracks. Since elongated manganese sulphide provides high stress concentration region, it is often considered the most detrimental of all. Liu *et al.* [14] showed that the crack initiation in pipeline steels considerably depends

*Corresponding author: m.mohtadi@bonabu.ac.ir

on the type and morphology of inclusions. These authors found two types of inclusion enriched with aluminum and silicon in the X70 specimen. Aluminum oxide inclusion was brittle and incoherent with the metal matrix and increased HIC susceptibility by being crack initiation site. However, hydrogen cracks did not nucleate around the silicon oxide inclusion due to its spherical morphology. Moore and Warga [15] showed that the morphology of manganese sulphide inclusions plays a key role in increasing HIC susceptibility in pipeline steel.

Various methods have been examined to improve the HIC resistance in pipeline steels. For instance, a lot of effort has been designated to substitute the detrimental hydrogen traps with the non-detrimental ones, control of morphology of inclusions, desulfurization of steel, control of nitrogen and carbon elements. However, such methods have not been sufficiently effective to prevent HIC cracks in pipeline steels. Beside these conventional methods, the crystallographic texture is considered as a new approach to prevent HIC crack propagation in pipeline steel. However, this method is completely new and there is a need for a lot of research to optimize the HIC resistance in pipeline steels. There are several studies showing that HIC resistance strongly depends on macro and micro-texture in pipeline steel. Venegas *et al.* [16] investigated the role of texture on HIC susceptibility in pipeline steel and concluded that there is a strong correlation between texture and HIC mitigation in pipeline steels. These authors showed that {111} dominant texture decreases the probability of crack coalescence and local plastic deformation of <111>//ND oriented grains reduces the probability of cracks propagation and deflection of cracks path towards the radial direction of the pipe. In another work, it has been shown that {111}, {110} and {112} dominant textures increase HIC resistance while {100} dominant texture increases HIC susceptibility by providing easy crack propagation path [17,18].

In this study, inclusions were categorized in X70 steel based on type and morphology. Role of each on HIC susceptibility was discussed. Finally, HIC cracks were analyzed based on the EBSD measurements.

2. EXPERIMENTAL PROCEDURE

2.1. SEM and EDS analysis on tested material

In this research, all experiments were carried out on the X70 pipeline steel. The chemical composition of this steel was shown in Table 1. Moreover, rolling, transverse and normal directions were abbreviated as RD, TD and ND, respectively. To begin the experiments, first, the surface of steel sheet (RD-TD plane) with the size of 20 (RD) × 20 (TD) mm was accurately polished with 120, 220, 320, 500, 600, 1200, 20000 and 4000 grit SiC emery papers and then 3 and 1 μm diamond paste was utilized to polish the same surface. When the polishing procedure was done, the polished surface was etched with 2% nital solution for 15 seconds. At this stage, the SEM observations was started to see the microstructure of X70 steel. SEM observations were carried out by using a SU6600 Hitachi field scanning electron microscope with an Oxford Instruments Nordlys nano EBSD detector. Moreover, the polished area was accurately checked to find out the inclusions. When the inclusions were found, the EDS analysis was used to predict their type.

2.2. Electrochemical hydrogen charging

Electrochemical hydrogen charging experiments were done in order to create HIC cracks in the X70 steel. To this, three specimens with the dimension of 130(TD)×25(RD)×9(ND) mm were cut from the as-received X70 steel sheet. Then, all surfaces were polished up to 600 grit emery paper. Before hydrogen charging, all specimens were washed with distilled water and then ultrasonically degreased with acetone for 30 minutes. Each specimen was separately put in a glass test vessel which was full with two liters of 0.2 M sulfuric acid and 3 g/l ammonium thiosyanate. An Instek type power supply was utilized to provide a constant current density of 20 mA/cm^2. The specimens were electrochemically charged with hydrogen for 8 hours. When charging process was done, each specimen was cut from the TD direction and the cross section of charged steel (RD-ND plane) was polished with 1 μm diamond paste at the final stage of polishing. In order to observe the HIC cracks by SEM and optical microscope (OM), the provided surfaces were etched with 2% nital solution.

2.3. EBSD measurements on HIC tested X70 steel

There is no need to etch the cross section of charged steel (RD-ND plane) with nital solution for EBSD measurements. However, when the RD-ND plane of charged specimen was polished with 1 μm diamond paste, the provided surface was vibrometery polished with 0.04 μm colloidal silica slurry for half day. After EBSD measurements, Oxford Instruments Channel 5 post processing software was used to analyze EBSD Raw data. It is worth-mentioning that EBSD measurements were done on HIC cracks in order to understand how crack propagates through the pipeline steel.

3. RESULTS AND DISCUSSION

3.1. Microstructure of as-received X70 steel

Figure 1 shows the microstructure of surface (RD-TD plane) of API X70 pipeline steel. The microstructure has been basically

Table 1. Chemical composition of API X70 pipeline steel (wt%)

Pipeline Steel	C	Mn	Si	Nb	Mo	Ti	Cr	Cu	Ni	V
X70	0.025	1.65	0.26	0.068	0.175	0.015	0.07	0.21	0.08	0.001

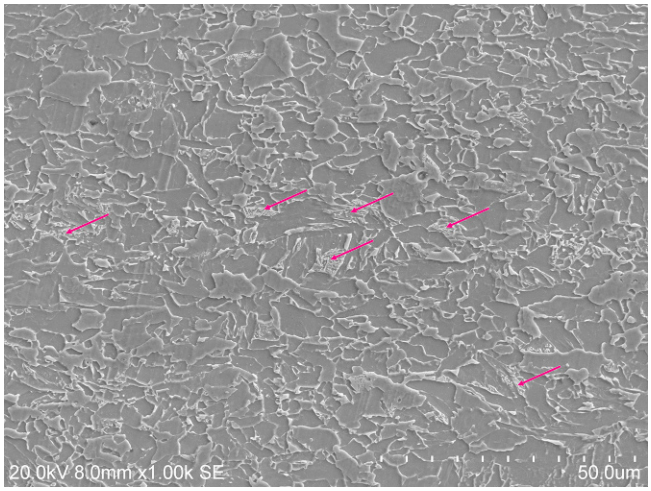

Fig. 1. SEM micrograph of microstructure of surface (RD-TD plane) of X70 pipeline steel.

composed of ferrite phase. A little fraction of area including pearlite structure is also seen in this microstructure which is shown with arrows. Since previous studies showed that HIC cracks are usually appeared at the center of cross section [17,18], the microstructure of this area is also investigated. The microstructure of the center of cross section of X70 steel is represented in Fig. 2(a). As it is clear, a high area fraction of microstructure of this section has been composed of ferrite. Also, a considerable amount of pearlite and small amount of martensite are also seen in Fig. 2(a). Figure 2(b) is one part of Fig. 2(a) with a higher magnification. This figure clearly confirms the presence of pearlite and martensite blades at the center of cross section of X70 steel. Two different phases including ferrite and cementite form the pearlite structure which is harder and more brittle than the ferrite. Martensite phase is the hardest and the most brittle phase which is present in the microstructure of this steel. This phases makes this area of X70 steel more susceptible to HIC than the other regions.

3.2. Effect of various microstructural parameters on HIC cracks

Many efforts have been designated to improve the quality of pipeline steel especially prevent HIC crack propagation. For instance, addition of some micro-alloying elements, such as addition of calcium, nickel and copper, is considered as an effective way to control the morphology of inclusions. Reducing sulfur content is another way that prevents the formation of detrimental manganese sulfide inclusion [19,20]. Applying protective film to the surface of pipeline in order to avoid the entrance of hydrogen atoms inside the structural defects is another method that can be considered to keep pipeline steels away from HIC cracks. It has been shown that the microstructure of steel plays an important role in HIC susceptibility [13]. In other words, the hard phases increase HIC susceptibility by facilitating the HIC crack propagation. Figure 3 shows SEM image of HIC crack which has been taken from the center of cross section of X70 steel. As shown in this Figure, an HIC crack propagates through different phases or structures. Figure 3(b), one part of Fig. 3(a) with a higher magnification, confirms that the HIC crack propagates through ferrite and pearlite phases. Actually, the hardness value of pearlite is higher than the ferrite and provides easy propagation path for HIC crack. It should be noted that the X70 pipeline steel composition indicates a very low carbon, high manganese steel strengthened by the carbonitride forming elements such as Nb, Mo and Ti. The low carbon content correlates with a low volume fraction of pearlite and the absence of the obvious pearlite banding found in hot rolled steels. Nevertheless, manganese segregation into bands is likely to be significant, and manganese-enriched regions will transform to ferrite at lower temperatures on cooling. A consequence is that the transformation

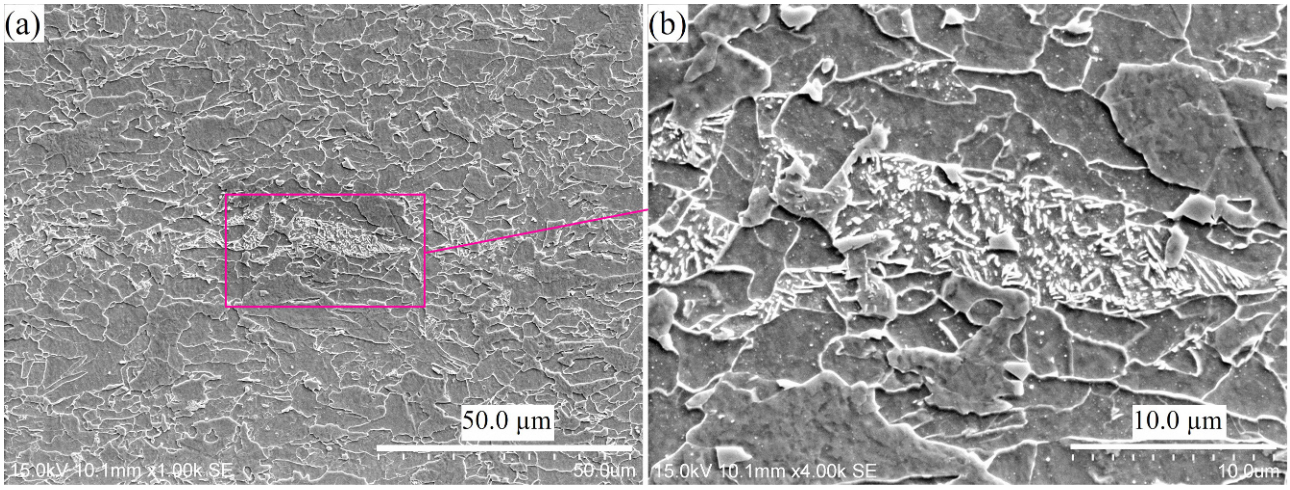

Fig. 2. SEM micrograph of microstructure of center of cross section (RD-ND plane) with (a) 1.00k magnification, (b) 4.00k magnification (Fig. 2(b) is one section of Fig. 2(a) with higher magnification).

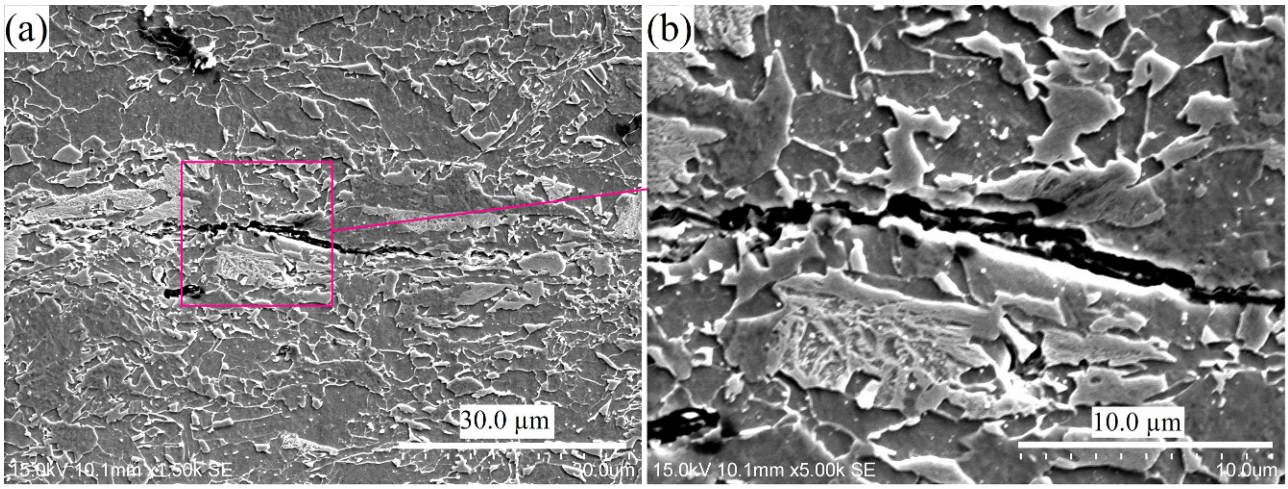

Fig. 3. SEM micrograph of HIC crack at the center of cross section (RD-ND plane) with (a) 1.50k magnification, (b) 5.00k magnification (Fig. 3(b) is one section of Fig. 3(a) with higher magnification).

volume change will be higher than in manganese-depleted regions and the ferrite will be more dislocated. During the manufacturing of hot rolled steels, such as X70 steel, some elements are rejected to the center part of cross section because of the different melting point with iron. These elements increases the hard phase formation temperature at the center of cross section. In other words, the hard phases are accumulated in this region in pipeline steel. If one measures the hardness value around the HIC crack, it is observed that it reaches up to 350 Vickers in some areas. This is in agreement with the results of Moon el. Al who showed the HIC crack propagates through hard phases in pipeline steel [21,22]. Aside the effect of hard phases, the present inclusions at the center part of cross section are considered as HIC crack initiation site. Jin *et al.* [23] showed that non-metallic inclusions nucleate HIC cracks in X100 steel. Figures 4(a) and 4(b) show OM images of HIC cracks in X70 steel. As shown in these figures, we observe that HIC cracks do not propagate necessarily through a straight line. However, the cracks propagate in a sinusoidal curve. This proves that there is an anisotropy of microstructure and in distribution of inclusions as well in this section of pipeline steel. Moreover, based on Figs. 4(a) and 4(b), one can see that many inclusions surrounded HIC cracks. Actually, the accumulation of inclusions in an especial region decreases the fracture toughness of that area and this makes that area highly susceptible to HIC. That is why we observe many inclusions around the HIC crack. The main deficiency of OM images is that it is not able to predict the type of inclusions. However, based on previous studies [18,6], some inclusions, such as manganese sulfide and carbonitride precipitates, have been found so detrimental to HIC phenomenon in pipeline steel. Figure 5(a) shows an inclusion around the center of cross section in as-received X70 steel which is incoherent with metal matrix. As clearly seen in this figure, the empty space between the inclusion and metal matrix provides suitable atmosphere for hydrogen atom concentration. Therefore, one may expect

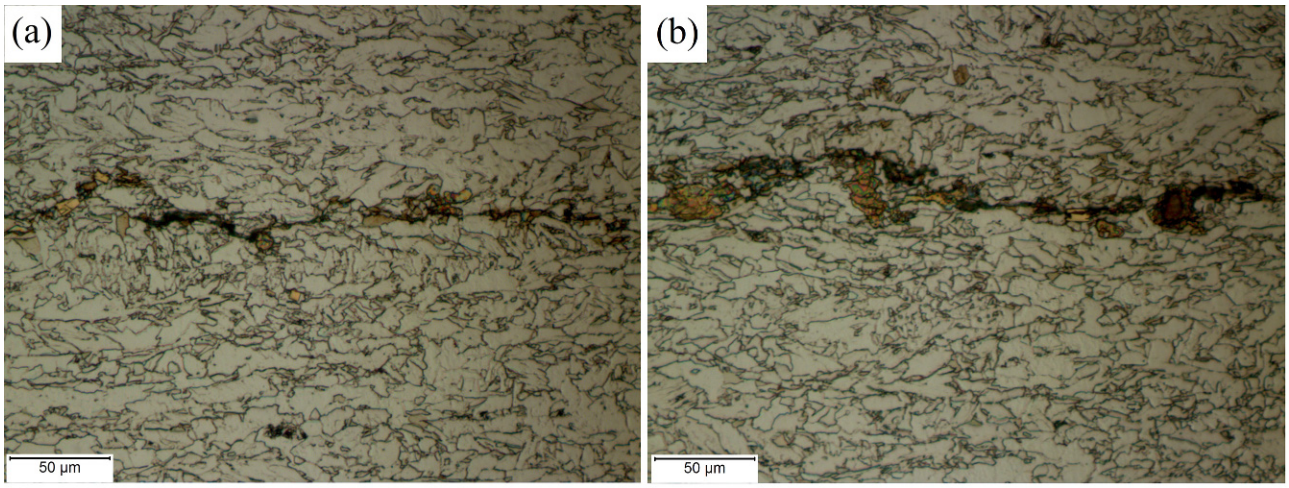

Fig. 4. OM micrograph of HIC crack at the center of cross section (RD-ND plane) in (a) region 1, (b) region 2.

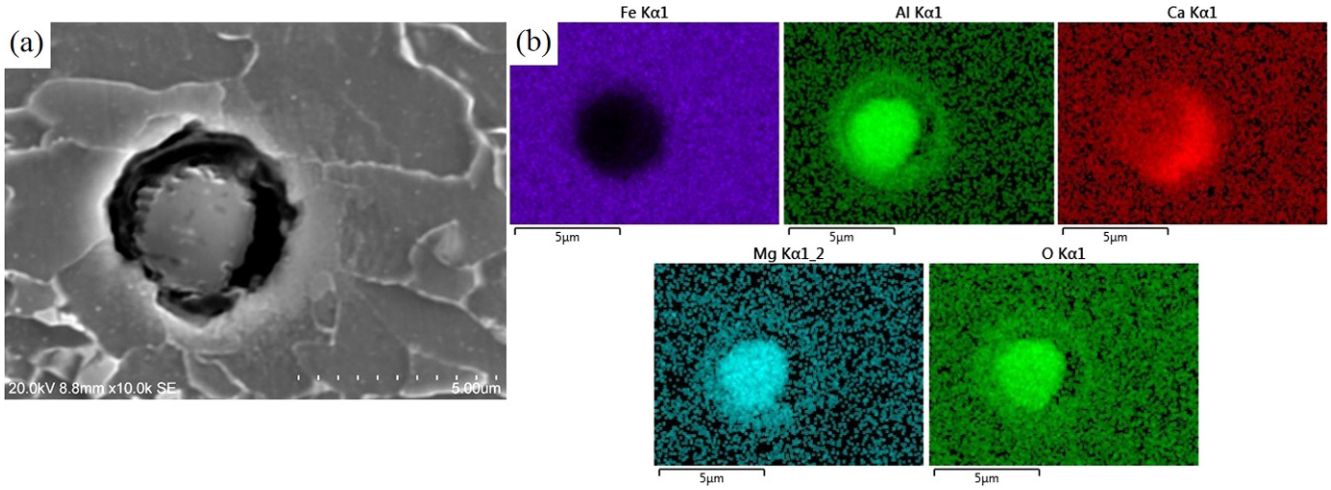

Fig. 5. (a) SEM micrograph of an inclusion, (b) EDS map scan on the inclusion showing Al-Ca-Mg oxide inclusion (The image was taken from the center segregation zone of API X70 pipeline steel).

that this inclusion may nucleate HIC crack. However, based on EDS map scan as shown in Fig. 5(b), the type of this inclusion is Al-Mg-Ca oxide inclusion. Aluminum oxide inclusion is hard and brittle and it is considered as crack initiation site. Hejazi *et al.* [13] studied HIC phenomenon in X70 pipeline steel and showed that this inclusion increases HIC susceptibility. However, we did not observe such inclusion to nucleate HIC crack after hydrogen charging. This may contradict with the findings of other researchers who showed that aluminum oxide inclusion may nucleate HIC crack. Here, there are two important points that should be considered. First, one can see that the calcium element has been added to this inclusion. As clearly seen in Fig. 5(b), calcium makes the shape of inclusion spherical and such inclusion cannot provide an area with high stress concentration factor. That is why we do not see this inclusion as HIC crack initiation site. Moreover, since calcium is a strong sulfide absorbent, it is added to steel to decrease the volume fraction of manganese sulfide. Figure 6(a) shows an elongated inclusion at center segregation zone in as-received X70 steel and EDS map scan, as shown in Fig. 6(b), confirms that the type of this inclusion is manganese sulfide. This type of inclusion is hard and brittle and is considered as HIC crack nucleation site [5,24]. Figure 7(a) shows a very complex inclusion at the center segregation zone in as-received X70 steel and based on the Fig. 7(b), its type is carbonitride precipitate plus Al-Mn-Ca oxide type inclusion. It is very interesting that the oxide inclusion with spherical shape has been mixed up with carbonitride precipitate with rectangular shape. This inclusion is so hard and brittle and may be considered as HIC crack nucleation site. It is notable that the morphology of this inclusion is almost spherical and it can apply stress concentration less than elongated manganese sulfide. Figures 8(a) and 8(b) show a pure elongated manganese sulfide with sharp edges at the center segregation zone in X70 steel. Its sharp edges can provide a very high stress concentration factor and nucleate HIC cracks easily. Sometime precipitates get an especial mor-

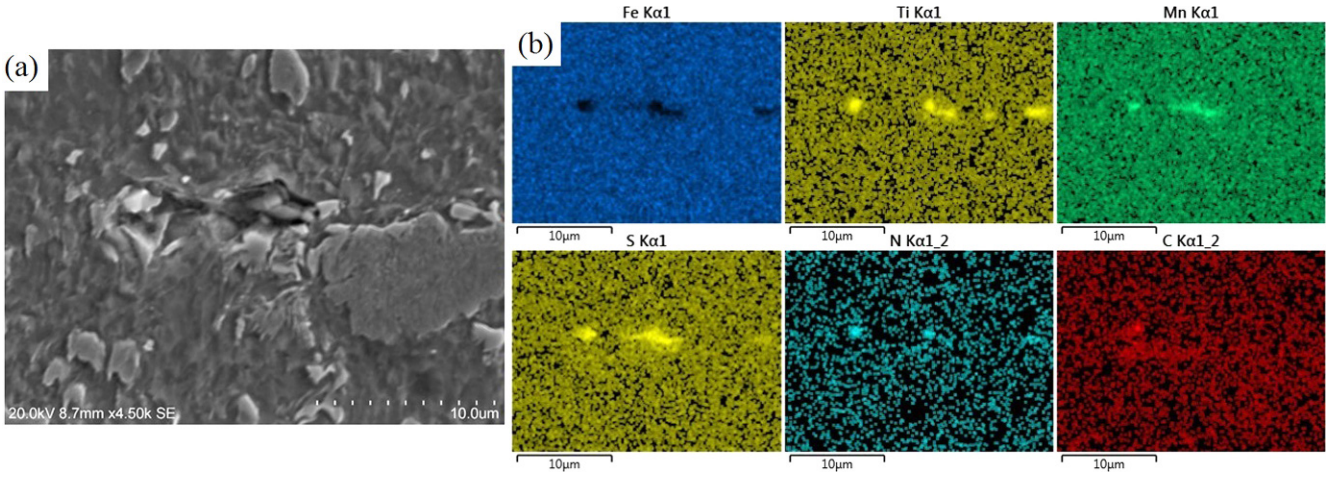

Fig. 6. (a) SEM micrograph of an inclusion, (b) EDS map scan on the inclusion showing manganese sulfide inclusion (The image was taken from the center segregation zone of API X70 pipeline steel).

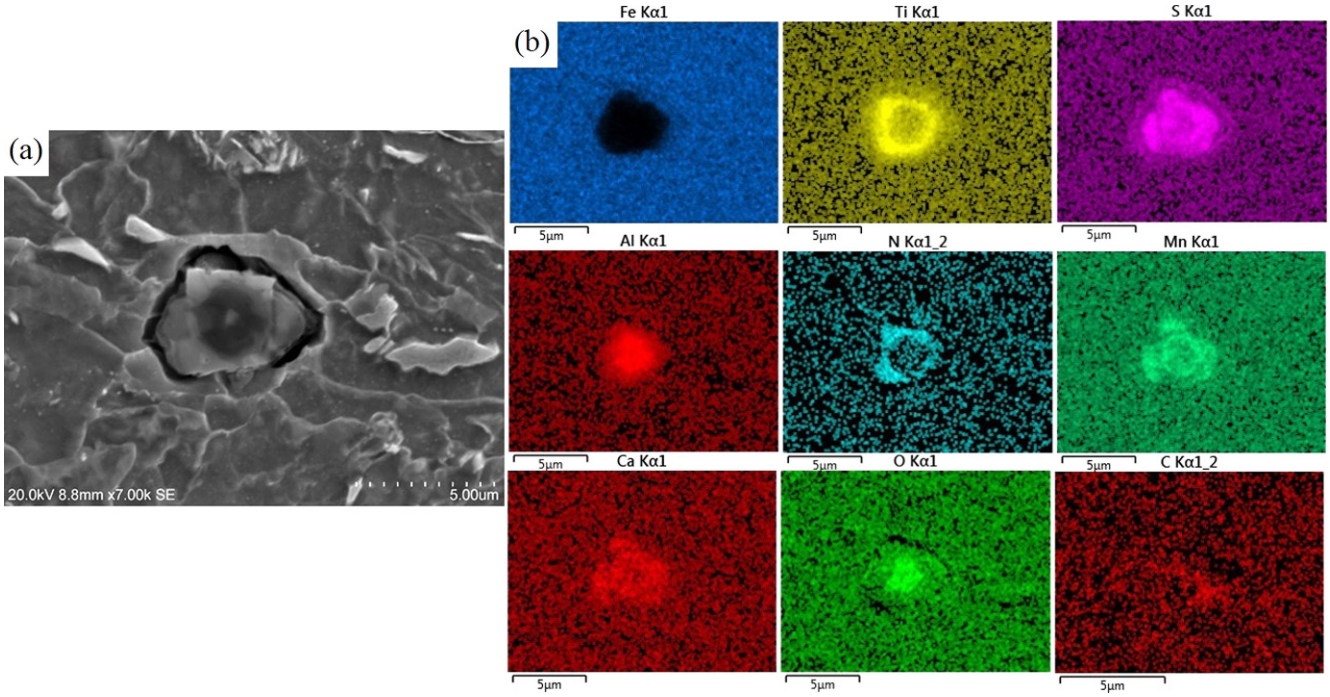

Fig. 7. (a) SEM micrograph of an inclusion, (b) EDS map scan on the inclusion showing manganese sulfide and carbonitride inclusion (The image was taken from the center segregation zone of API X70 pipeline steel).

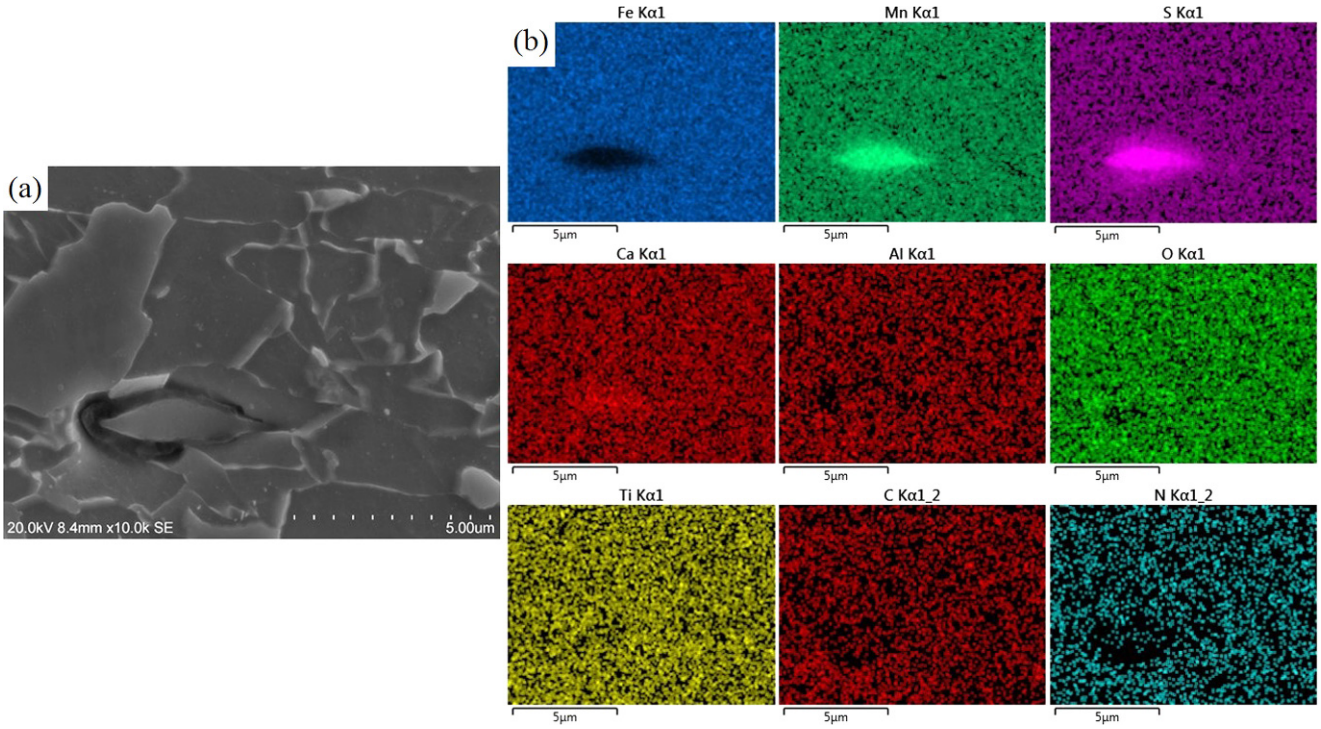

Fig. 8. (a) SEM micrograph of an inclusion, (b) EDS map scan on the inclusion showing manganese sulfide inclusion (The image was taken from the center segregation zone of API X70 pipeline steel).

phology. For instance, if one look at Fig. 9, the type of this precipitate is nitride and its morphology is rectangular. Even though this type of inclusion have very sharp edges that can provide high stress concentration regions, it is coherent with metal matrix. Therefore, due to its coherency, it may not nucleate HIC crack. Up to now, we discussed role of each type of inclusion in HIC phenomenon. It is worth-mentioning that the morphology of precipitates is not the sole determinant of their

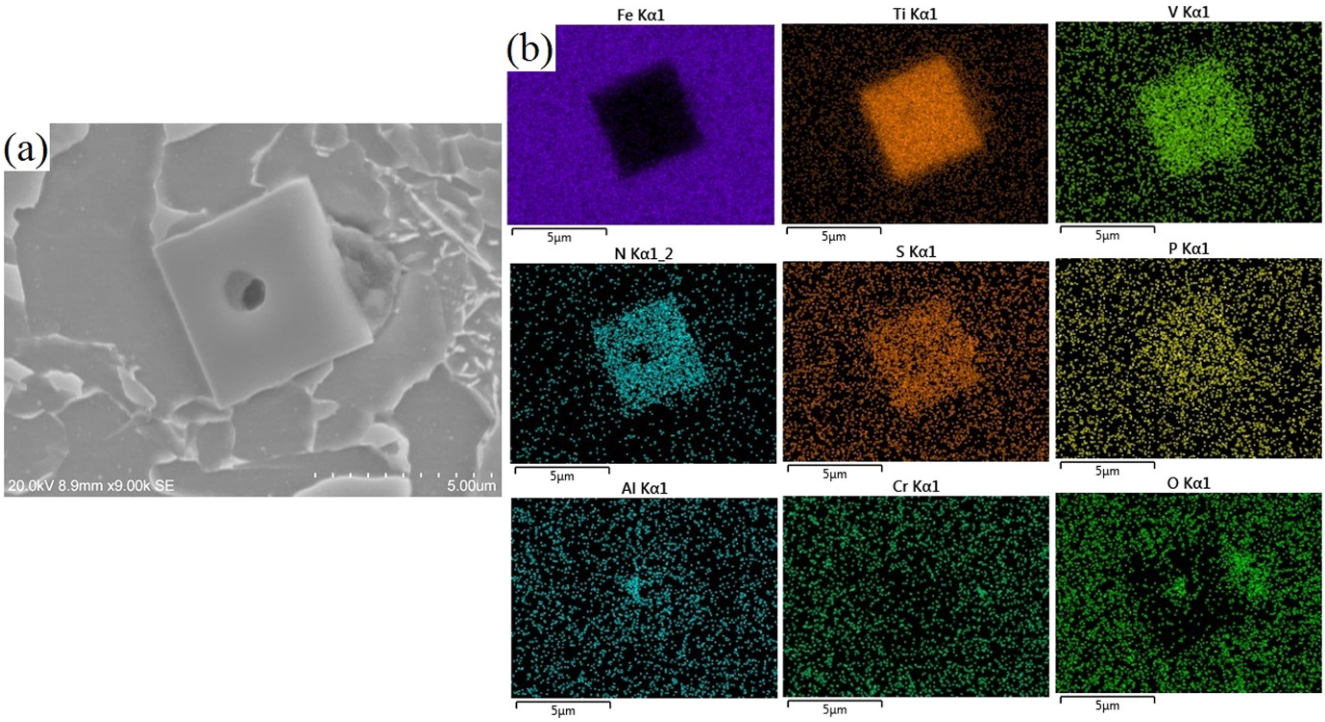

Fig. 9. (a) SEM micrograph of an inclusion, (b) EDS map scan on the inclusion showing nitride inclusion (The image was taken from the center segregation zone of API X70 pipeline steel).

HIC susceptibility. Spherical particles can also induce HIC cracking by interfacial decohesion, promoted by hydrogen concentration in the region surrounding the particle where plastic and elastic strains are present. Moreover, there are many reports showing spherical oxide particles along the paths of hydrogen induced cracks. Another important factor that should be considered is the microstructure and distribution of inclusions around the HIC crack. As shown in Fig. 10, there is a HIC crack that have been generated after 8 h electrochemical hydrogen charging. One can see several types of inclusions that appeared at the crack propagation path. More probably, there has been HIC crack nucleation site. More importantly, there are some types of inclusions around both sides of HIC crack. Moreover, it is seen some pearlite structure around the HIC crack. These inclusions and hard structures decreased the fracture toughness of this region and made this area more susceptible to HIC. In this study, 60 different inclusions were investigated in hydrogen charged X70 steel. Statistically, 70% of these inclusions were from oxide type including Al-Ca-Mg-Mn, 12% were from sulfide type including Mn, and rest of them were from carbonitride type including Ti-V-Nb-C-N. In some cases, mixed type of inclusions, such as carbonitride precipitate and manganese sulfide, were found. Moreover, some of inclusions were not pure. For instance, if one refers to Fig. 6, it is seen that there is Ti element on manganese sulfide inclusion.

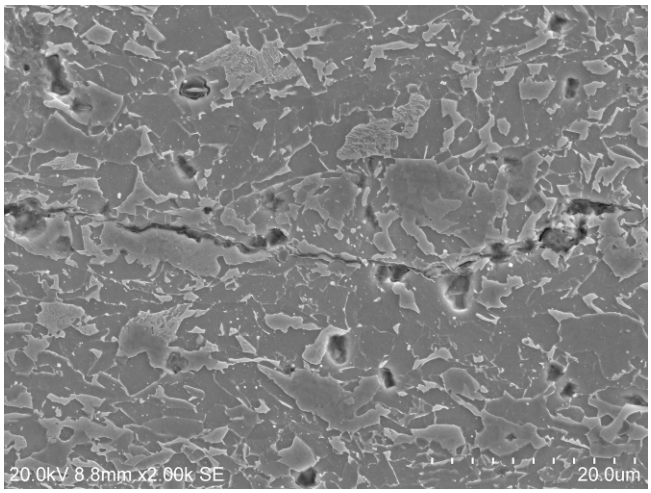

Fig. 10. SEM micrograph of HIC crack at the center of cross section (RD-ND plane) and different types of inclusions around the crack.

3.3. EBSD measurement on HIC propagation path

Beside the effect of microstructure and inclusions on HIC crack propagation, crystallographic texture plays an important role in HIC crack propagation. Crystallographic texture and grain boundary engineering are considered as innovative techniques to improve HIC resistance in pipeline steel. To investigate the role of micro-texture on HIC crack propagation, EBSD measurement on several HIC crack has been carried out. In the literature [16,19], it has been implied that all HIC cracks initiate from structural defects, such as inclusions and precipitates, and propagate through the rolling direction. This is the

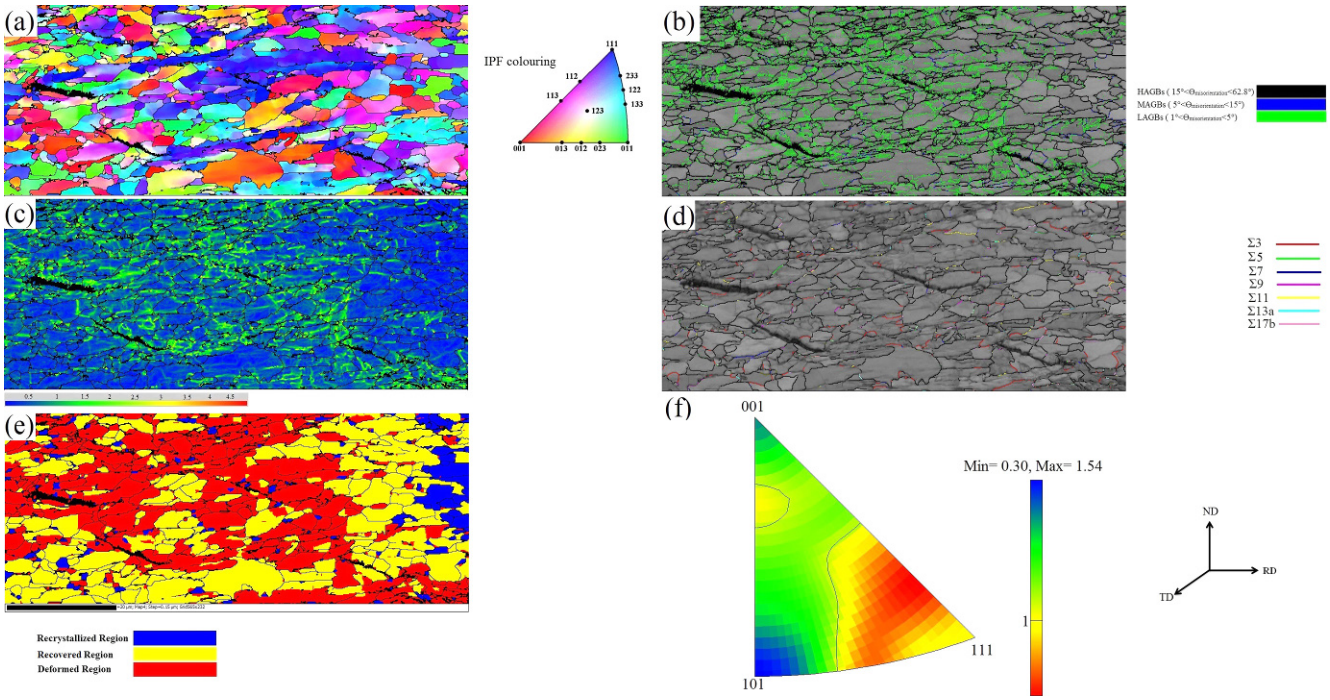

Fig. 11. EBSD constructed (a) inverse pole figure map, (b) grain-boundary map, (c) KAM map, (d) coincidence site lattice (CSL) boundaries, (e) recrystallization fraction map, and (f) inverse pole figure in hydrogen charged X70 steel.

region where center segregation of some elements, such as carbon and manganese, occurs. In this research, we observed a different type of HIC crack which has a deviation from the rolling direction. Based on Fig. 11(a), IPFz map around several HIC cracks, it is observed that several small HIC cracks propagate not exactly in the rolling direction but with several degrees of deviation (15-20 degrees) with respect to the rolling direction. Since HIC cracks propagate along the easiest path available to it, which normally involves grain boundaries and boundaries between precipitates and matrix, this deviation can be justified. The reported deviations of the HIC crack path by up to about 20 degrees from the rolling direction is consistent with this premise. In this work, we did not apply any external stress during HIC testing. Figure 11(a) shows that the HIC cracks propagated by stepwise manner. In our previous work [9], when external stress was applied during HIC testing, there was not observed any stepwise cracking. This is also with good agreement with findings of Iino [27] who showed that crack propagation occurs by stepwise linking of small cracks in the absence of the external stress. As shown in Fig. 11(a), since the cracks propagated between grains with different orientations, the dominant mode of HIC cracks is intergranular. It is notable that both types of inter and trangranular cracking may occur in HIC phenomenon. However, the type of these cracks strongly depends on the type of grains, type of grain boundaries and local microstructure of the region surrounded HIC crack [18]. Considering Fig. 11(a), we observe that the dominant mode for HIC crack propagation is transgranular and HIC crack propagated in intergranular manner only in a few cases. The orientation of grains is also important in HIC crack propagation. One can see in Fig. 11(a) that the local texture of the EBSD measured area is weak. Therefore, the weak local texture is supposed to facilitate HIC crack propagation. Therefore, one can conclude that HIC cracks propagate dominantly in transgraular manner through differently oriented grains and it was not observed any clear preferential trend. The type of grain boundaries around the HIC cracks is shown in Fig. 11(b). We defined the grain boundaries with misorientation of $1°<\theta<5°$, $5°<\theta<15°$ and $15°<\theta<62.8°$ as low angle grain boundaries (LAGBs), medium angle grain boundaries (MAGBs) and high angle grain boundaries (HAGBs), respectively. In this figure, the LAGBs, MAGBs and HAGBs were shown with green, blue and black colors. As shown in Fig. 11(b), in some cases, the HIC cracks have been arrested in green regions which has a low angle grain boundary. Therefore, low angle grain boundaries are able to increase HIC resistance by stopping HIC cracks. Figure 11(b) clearly shows that dislocations have been accumulated around the HIC cracks. Based on this figure, due to the accumulation of dislocations around the HIC crack, we expect that the (Kernel Average Misorientation) KAM value around the HIC crack should be higher than other regions, see Fig. 11(c). It is worth-mentioning that KAM shows the average misorientation between a point inside a grain and its neighbors inside the same grain [25]. Figure 11(c), KAM map, also confirms that the plastic deformation mainly occurred around the HIC crack propagation path. However, here, two

strategies can be considered for crack propagation. First, some of such deformation was happened during the hot rolling in manufacturing process. Second, rest of deformation was occurred during the crack propagation. The main point is that the stored energy of deformation of this area was high enough to be potentially ready for HIC crack propagation. Distribution of coincidence site lattice (CSL) boundaries around the HIC cracks was shown in Fig. 11(d). The CLS boundaries are considered as low angle grain boundaries and are resistant for intergranular HIC crack propagation. Based on Fig. 11(d), the discussion about the role CLS boundaries on HIC crack propagation is speculative; however, one may see the accumulation of Σ3 on the EBSD measured area. First, the fraction of Σ3 boundaries compared with other boundaries is high. Moreover, it has been implied that Σ3 boundaries are categorized as HAGBs because twining does not occur in Σ3 type boundaries in pipeline steel [26]. This is one possible reason that this type of boundary may increase the propagation of intergranular HIC crack. Figure 11(e) shows the recrystallization map in which the recrystallized, recovered and deformed regions were shown with blue, yellow and red colors, respectively. EBSD uses the grain orientation spread (GOS) method which can recognize a recrystallized grain among several plastically deformed grains. When the GOS value of a grain is less than 2°, it is identified as a recrystallized grain. However, when the GOS value of a grain varies between 2° and 4°, it is recognized as a recovered grain. Finally, the GOS value for a deformed grain is over 4°. This method calculates the average orientation of each grain and then compares the misorientation of each pixel in the grain from its average to determine the average orientation spread. As it is clear, the stored energy of deformation for a deformed grain is higher than that in recrystallized and recovered grains. That is why we observe that the HIC cracks propagate through the deformed grains. It is notable that some of these grains were deformed during the hot rolling and full recrystallization was not gained during hot deformation. The inverse pole figure for the EBSD measured area was shown in Fig. 11(f). Even though the inverse pole figure shows that the dominant local texture of the measured area is {111}, the intensity of this inverse pole figure is very low (1.54) and the texture of this area should be supposed as a weak texture. It has been implied that pipeline steels with {111}, {112} and {110} dominant textures reduces the probability of HIC crack by reducing the number of inter and transgraular low resistance cleavage paths [16].

4. CONCLUSION

We obtained the following results on as-received and hydrogen charged API X70 pipeline steel:

(1) Different type of inclusions were found at the cross section of as-received X70 pipeline steel. Among these, due to the type and morphology, manganese sulphide and carbonitride precipitate were found detrimental to HIC cracks.

(2) Oxide inclusions do not initiate any HIC crack in X70 pipeline; however, they decrease the fracture toughness of local area and increase HIC susceptibility.

(3) Several HIC cracks were investigated and it was concluded that they propagated through differently oriented grains; however, the dominant textures around the HIC cracks were random.

(4) In X70 pipeline steel, HIC cracks propagate dominantly in transgraular manner through differently oriented grains with no clear preferential trend.

(5) Recrystallization map showed that the cracks propagated through the deformed grains. These grains with high levels of stored energy are highly prone to HIC cracking. Some of the grains were deformed during the HIC crack propagation.

ACKNOWLEDGMENT

We would like to thank the Research Center of University of Bonab for the financial support of this project.

REFERENCES

1. R. A. Oriani and P. H. Josephic, *Acta Metall.* **27**, 997 (1979).
2. C. A. Zapffe and C. E. Sims, *T. Am. I. Min. Met. Eng.* **145**, 225 (1941).
3. A. S. Tetelman and W. D. Robertson, *T. Am. I. Min. Met. Eng.* **224**, 775 (1962).
4. M. A. Mohtadi-Bonab, J. A. Szpunar, and S. S. Razavi-tousi, *Eng. Fail. Anal.* **33**, 163 (2013).
5. M. A. Mohtadi-Bonab, J. A. Szpunar, L. Collins, and R. Stankiewich, *Int. J. Hydrogen Energ.* **39**, 6076 (2014).
6. M. A. Mohtadi-Bonab, J. A. Szpunar, and S. S. Razavi-tousi, *Int. J. Hydrogen Energ.* **38**, 13831 (2013).
7. X. B. Shi, W. Yan, W. Wang, L. Y. Zhao, Y. Y. Shan, and K. Yang, *J. Iron Steel Res. Int.* **22**, 937 (2015).
8. Z. Y. Liu, X. Z. Wang, C. W. Du, J. K. Li, and X. G. Li, *Mat. Sci. Eng. A* **658**, 348 (2016).
9. M. A. Mohtadi-Bonab, M. Eskandari, K. M. M. Rahman, R. ouellet, and J. A. Szpunar, *Int. J. Hydrogen Energ.* **23**, 4185 (2016).
10. M. A. Mohtadi-Bonab, R. Karimdadashi, M. Eskandari, and J. A. Szpunar, *J. Mater. Eng. Perform.* **25**, 1781 (2016).
11. T. Hara, H. Asahi, and H. Ogawa, *Corros. Sci.* **60**, 1113 (2004).
12. W. K. Kim, S. U. Koh, B. Y. Yang, and K. Y. Kim, *Corros. Sci.* **50**, 3336 (2008).
13. D. Hejazi, A. J. Haq, N. Yazdipour, D. P. Dunne, A. Calka, F. Barbaro, *et al. Mat. Sci. Eng. A* **551**, 40 (2012).
14. Z. Y. Liu, X. G. Li, C. W. Du, L. Lu, Y. R. Zhang, and Y. F. Cheng, *Corros. Sci.* **51**, 895 (2009).
15. E. M. Moore and J. J. Warga, *Mater. Performance* **15**, 17 (1976).
16. V. Venegas, F. Caleyo, T. Baudin, J. H. Espina-Hernández, and J. M. Hallen, *Corros. Sci.* **53**, 4204 (2011).

17. M. A. Mohtadi-Bonab, M. Eskandari, and J. A. Szpunar, *Mat. Sci. Eng. A* **620**, 97 (2015).
18. M. A. Mohtadi-Bonab, J. A. Szpunar, R. Basu, and M. Eskandari, *Int. J. Hydrogen Energ.* **40**, 1096 (2015).
19. H. Tamehiro, T. Takeda, S. Matsuda, K. Yamamoto, and N. Okumura, *T. Iron Steel I. Jpn*. **25**, 982 (1985).
20. M. A. Al-Anezi and S. Rao, *J. Fail. Anal. Preven.* **11**, 385 (2011).
21. J. Moon, C. Park, and S. J. Kim, *Met. Mater. Int.* **18**, 613 (2012).
22. J. Moon, S. J. Kim, and C. Lee, *Met. Mater. Int.* **19**, 45 (2013).
23. T. Y. Jin, Z. Y. Liu, and Y. F. Cheng, *Int. J. Hydrogen Energ.* **35**, 8014 (2010).
24. J. Maciejewski, *J. Fail. Anal. Preven.* **15**, 169 (2015).
25. R. Badji, T.Chauveau, and B.Bacroix, *Mat. Sci. Eng. A* **575**, 94 (2013).
26. V. Venegas, F. Caleyo, J. M. Hallen, T. Baudin, and R. Penelle, *Metall. Mater. Trans. A* **38**, 1022 (2007).
27. M. Iino, *Metall. Mater. Trans. A* **9**, 1581 (1978).